JVSTB Journal of Vacuum Science & Technology B

Ultrahigh luminescence extraction via the monolithic integration of a light emitting active region with a semiconductor hemisphere

S.-N. Wu, S.-Q. Yu, D. Ding, S. R. Johnson, and Y.-H. Zhang

Citation: Journal of Vacuum Science & Technology B **29**, 031213 (2011); doi: 10.1116/1.3592190
View online: http://dx.doi.org/10.1116/1.3592190
View Table of Contents: http://scitation.aip.org/content/avs/journal/jvstb/29/3?ver=pdfcov
Published by the AVS: Science & Technology of Materials, Interfaces, and Processing

Ultrahigh luminescence extraction via the monolithic integration of a light emitting active region with a semiconductor hemisphere

S.-N. Wu,[a] S.-Q. Yu,[b] D. Ding, S. R. Johnson, and Y.-H. Zhang[c]
Center for Photonics Innovation, School of Electrical, Computer and Energy Engineering, Arizona State University, Tempe, Arizona 85287

(Received 11 January 2011; accepted 28 April 2011; published 31 May 2011)

A light emitting active region with three InGaAs quantum wells is monolithically integrated with a GaAs hemisphere as a means to increase the extraction efficiency of light emitting diodes. For a device with a small active region and large hemisphere and optimal antireflection, theoretical calculations show that the extracted fraction of spontaneous emission incident on the hemisphere is greater than 99.9% and the overall extraction efficiency of the integrated device is as high as 90%. The hemisphere is fabricated with a consistent aspect ratio (height versus width) using photoresist reflow and inductive coupled plasma etching. Detailed numerical simulations are performed to predict the reflow and dry etch processes as an aid to device fabrication. The fabrication results show that near perfect GaAs hemispheres can be successfully integrated with light emitting active regions and that the resulting light emitting diodes have the potential for mass production. © *2011 American Vacuum Society.* [DOI: 10.1116/1.3592190]

I. INTRODUCTION

High efficiency semiconductor light emitting devices are desirable for solid state lighting, large area displays, optical communications, and sensing applications. Both high internal quantum efficiency and high extraction efficiency are necessary to attain high performance. Furthermore, if the overall energy conversion efficiency of light emitting diodes (LEDs) exceeds 100%, namely, the total photon energy extracted is greater than the electrical input, then it is possible to achieve electroluminescence cooling.[1,2] Luminescence based coolers are vibration-free and capable of much lower operating temperatures than conventional thermoelectric coolers,[2,3] which makes them ideal for space applications.

Although photoluminescence refrigeration has been realized in doped glass and doped crystal materials using laser pumping,[4–6] this effect has not been observed in semiconductor devices. One of the major challenges to the realization of electroluminescence refrigeration in LEDs is that the energy conversion efficiency is limited by poor light extraction caused by the large difference in the indices of refraction between semiconductors and air. For example, due to light trapping, a planar GaAs structure emits approximately 2% of the internally generated spontaneous emission into free space through a given surface. Moreover, many advanced structures have been utilized to enhance light extraction, such as epoxy encapsulation, photonic crystals, and surface roughening;[7–9] notwithstanding these efforts, the extraction efficiency in LEDs is still far from unity.

In order to further enhance light extraction, we have monolithically integrated a transparent semi-insulating GaAs hemisphere with a light emitting active region containing three InGaAs/GaAs quantum wells; in a previous work, a similar active region demonstrated a spontaneous emission quantum efficiency of 94% at room temperature and over 99% at 100 K.[10] When optimized, the primary function of this design is the elimination of light trapping within the device, which greatly reduces losses related to photon recycling in the active region and parasitic absorption caused by free carriers and metal contacts. Moreover, since the emission from the InGaAs quantum wells (980 nm) is well below the bandgap energy of GaAs, the absorption losses in the semi-insulating GaAs hemisphere are negligible.

II. DEVICE STRUCTURE AND SIMULATIONS

A schematic diagram of an antireflection coated semiconductor hemisphere monolithically integrated with a light emitting active region is shown in Fig. 1. In this structure, the interface reflection between the active region and the hemisphere is negligible because the respective refractive indices are very closely matched. Contrary to planar structures, a hemisphere device can be designed so that all of the spontaneous emission that falls onto a given point of the hemisphere-air interface lies within the escape cone provided the hemisphere diameter is sufficiently larger than the active region diameter.

First, the largest usable incident angle within the escape cone at the hemisphere-air interface is determined. Using the law of cosines, as shown in Fig. 1, the incident angle α can be expressed as

$$\cos(\alpha) = \frac{R^2 + L^2 - r^2}{2RL}, \tag{1}$$

where R is the radius of the hemisphere, r is the radial distance from the center to a given point on the surface of the active region, and L is the distance from the corresponding

[a]Present address: 1534 Ambergrove Dr., San Jose, CA, 95131.
[b]Present address: Department of Electrical Engineering, University of Arkansas, Fayetteville, AR,72701.
[c]Author to whom correspondence should be addressed; electronic mail: yhzhang@asu.edu

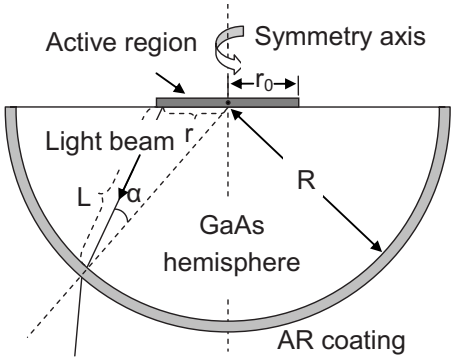

FIG. 1. Schematic of the hemisphere structure for highly efficient light extraction.

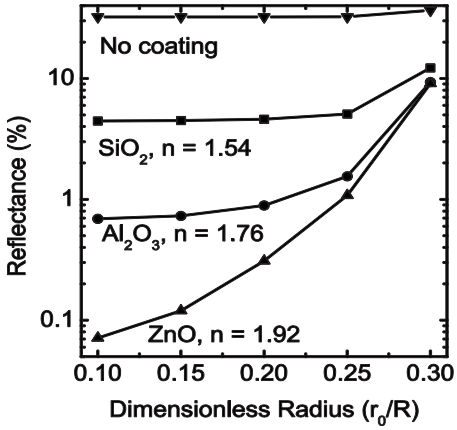

FIG. 2. Internal reflectance of GaAs hemisphere with various antireflection coatings for spontaneous emission from InGaAs active regions with different radii.

point on the active region surface to the hemisphere surface. The incident angle goes through a maximum at $L^2=R^2-r^2$, which occurs when light is emitted perpendicular to the surface of the active region, with $\sin(\alpha)=r/R$. Furthermore, the condition for total internal reflection is given by $\sin(\alpha)>1/n$, where n is the refractive index, and since the maximum value of r is the active region radius r_0, then as long as $R>nr_0$, all of the spontaneous emission from the active region falls within the escape cone. Moreover, due to the small incident angles, an effective antireflection coating is relatively easy to attain.

A. Simulation of luminescence extraction

As shown in Fig. 1, the device consists of a thin light emitting disk (active region) integrated with a semiconductor hemisphere in a design that enhances light extraction. To evaluate the performance of this design, the extracted fraction of the spontaneous emission leaving the active region on the hemisphere side is calculated for various hemisphere sizes with single-layer antireflection coatings. It is assumed that the light over the entire active region emission spectrum is randomly polarized and uniformly distributed in all directions. Furthermore, in the case where the hemisphere is large enough to eliminate light trapping, the only backreflection is due to a less than ideal antireflection coating on the hemisphere surface. As a worst case scenario, the reflected light is assumed to be parasitically lost inside the hemispherical device. This assumption underestimates the performance as part of the reflected light is extracted as it again reaches the hemisphere surface through multiple reflections.

The calculations are performed using the transfer matrix method.[11] Since plane waves are utilized in this method, the hemisphere surface is approximated by many small flat areas in the calculation. In the calculations, single-layer antireflection coatings are chosen using the materials SiO_2, Al_2O_3, and ZnO with refractive indices 1.54, 1.76, and 1.92, respectively.[12–14] The refractive indices are assumed to be constant in energy due to the narrow spectral width of the quantum well emission. The ratio of the active region radius to the hemisphere radius is defined as the dimensionless radius, r_0/R, that is varied from 0.10 to 0.30. For a given dimensionless radius and antireflection coating material, the coating thickness is optimized to minimize the reflectance at the hemisphere-air interface over the entire emission spectrum.

The results are shown in Fig. 2, where the reflectance loss increases dramatically when the dimensionless radius exceeds 0.25, which is the ratio where the onset of total internal reflection occurs as some of the emitted light lies outside of the escape cone. Moreover, ZnO provides the lowest reflectance among the three materials studied due to its higher refractive index. For large hemispheres with a small dimensionless radius (<0.15) and proper ZnO antireflection coating, the reflectance loss is less than 0.1%, which is negligible compared to the other losses in the device; in which case the hemisphere is essentially a perfect extractor.

The extraction efficiency for the entire LED structure can be written as

$$\eta_e = \frac{\text{Extraction factor}}{\text{Extraction factor} + \text{Loss factor}} = \frac{1 - \text{Loss factor} - \text{Recycling factor}}{1 - \text{Recycling factor}}, \quad (2)$$

where the extraction factor is the fraction of the active region spontaneous emission that is extracted from the spherical surface of the hemisphere, the loss factor is the fraction of the spontaneous emission lost to internal parasitic absorption plus the fraction extracted from the flat surface of the hemisphere, and the recycling factor is the fraction of the spontaneous emission that is absorbed in the active region, which is not a loss from the standpoint of extraction efficiency as the photon energy is recycled.

Next, the extraction factor and the extraction efficiency are determined by estimating the loss factor and recycling factor. Free carrier absorption, which typically has an absorption coefficient less than 50 cm^{-1}, results in a parasitic loss that is less than 1%.[15] The parasitic losses caused by free carrier absorption are greatly reduced in this device design because the hemisphere effectively eliminates trapped light; a substantial improvement over a planar design where light

TABLE I. Fraction of spontaneous emission lost, recycled, and extracted, and the resulting extraction efficiency.

	Design 1	Design 2
Fraction of active region covered by contact	44%	22%
Spontaneous emission absorbed by metal contact	16%	8%
Spontaneous emission extracted from flat side of hemisphere	1%	1%
Spontaneous emission absorbed by free carriers	1%	1%
Spontaneous emission recycled	4%	4%
Spontaneous emission extracted from hemisphere	78%	86%
Extraction efficiency	81%	90%

trapping results in multiple passes through the device regions containing free carriers before extraction occurs.

However, absorption in metal contacts adjacent to the active region can result in even larger parasitic losses than those for free carriers, particularly when the contact covers a significant portion of the active region. For example, the typical contact materials for GaAs consist of Ti/Pt/Au metal layers about 20/20/200 nm thick; with a complex index of refraction coefficient of $3.03+3.65i$ at 980 nm,[13] about 72% of the incident light is absorbed by the Ti metal layer. In designing the size of a contact there is a trade-off between how well the current is spread (larger is better) and the absorption losses (smaller is better). Therefore, two contact designs are considered: in design 1, the contact offers good current spreading and covers 44% of the active region, and in design 2, the contact offers reduced current spreading and covers 22% of the active region. The loss is about 16% $(0.72\times0.44\times1/2)$ for design 1 and about 8% for design 2; note that only one-half of the spontaneous emission is incident on the contact, hence the 1/2 factor.

For the remaining 56% (or 78%) of the active region not covered by contacts, a small amount of the incident light is extracted from the flat side of the hemisphere through the escape cone containing about 4% of the incident spontaneous emission, of which 31% is reflected back; resulting in a loss that is less than 1% $(0.56\times0.04\times0.69\times1/2)$ for design 1 and about 1% $(0.78\times0.04\times0.69\times1/2)$ for design 2. Combining the three losses, the total loss factor is about 18% for design 1 and 10% for design 2. The photon recycling factor (fraction of spontaneous emission absorbed in the quantum wells) is approximately 4% using an absorption coefficient of 13 440 cm^{-1} for InGaAs.[12] Subtracting both the loss and recycling factors the extraction factor is 78% for design 1 and 86% for design 2. Note that both the loss and the recycling factors are greatly reduced in this device via the elimination of light trapping. From Eq. (2), this results in extraction efficiencies of 81% for a contact with 44% coverage (design 1) and 90% for a contact with 22% coverage (design 2). These results are summarized in Table I.

B. Photoresist reflow simulation

In order to fabricate a perfect GaAs hemisphere, a unique combination of a photoresist mask and dry etch recipe is essential. Therefore, detailed numerical simulations are performed to predict the processing results as a guide to the experimental work. Measurements from a scanning electron microscope and profilometer are used to fine tune the theoretical simulations.

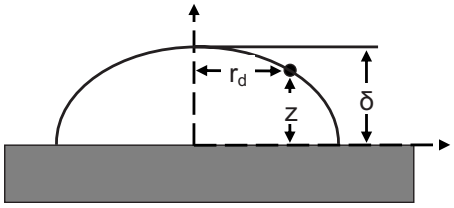

FIG. 3. Schematic diagram of a photoresist droplet on a flat surface.

The simulations consist of two parts: (i) a photoresist reflow simulation and (ii) an inductively coupled plasma (ICP) etch simulation. In order to fabricate a spherical semiconductor surface, a dome shaped photoresist mesa is utilized as a mask. Which is achieved by defining a cylindrical photoresist mesa using conventional photolithography, then heating up the photoresist and letting it reflow to take on a dome shape. After the reflow process, the volume is reduced roughly by 20% and the radius remains the same.

The shape of the curvature of the photoresist mesa dome after reflow is governed by the Young–Laplace equation,

$$\Delta p = \sigma\left(\frac{1}{R_1}+\frac{1}{R_2}\right), \tag{3}$$

where the photoresist is assumed to be a liquid droplet at steady state, Δp is the pressure difference across the photoresist-air interface, R_1 and R_2 are the principal radii of curvature at the interface, and σ is the surface tension coefficient of the droplet. A schematic diagram of the photoresist droplet is shown in Fig. 3. Following Eq. (3), the equation for a droplet at position (r_d,z) on a flat surface is written as

$$K(r_d) = K_0 + \frac{\rho g}{\sigma}[\delta - z(r_d)], \tag{4}$$

where

$$K(r_d) = -\left\{\frac{\frac{d^2z}{dr_d^2}}{\left[1+\left(\frac{dz}{dr_d}\right)^2\right]^{1.5}} + \frac{\frac{dz}{dr_d}}{r_d\left[1+\left(\frac{dz}{dr_d}\right)^2\right]^{0.5}}\right\}, \tag{5}$$

is the position dependent curvature of the free surface of the droplet,[16] $R_0=2/K_0$ is the radius of surface curvature at the apex, r_d is the radial distance, z is the height, δ is the droplet height at the apex, $\rho=1.08$ g/cm^3 is photoresist density,[17] and g is acceleration of gravity. In Eq. (4), the second term is at least two orders of magnitude smaller than the first one, because the surface tension coefficient normally ranges from 10 to 400 mN/m^2 and the droplet radius is around 100 μm.[18] Therefore, the accuracy of surface tension coefficient is not important and that of water (100 mN/m^2) is used in the calculation. Therefore, Eq. (4) can be written as

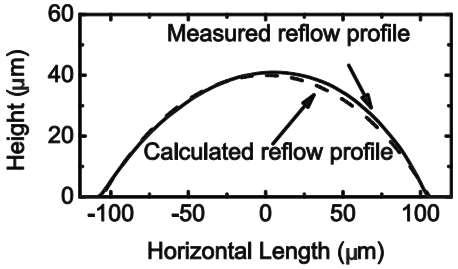

FIG. 4. Calculated (dashed curve) and measured (solid curve) photoresist droplet profile after reflow.

$$\begin{cases} dz/dr_d = y \\ dy/dr_d = -(1+y^2)^{1.5} \cdot \left[K_0 + \dfrac{\rho g}{\sigma}(\delta - z) \right] - \dfrac{y(1+y^2)}{r_d} \end{cases}, \tag{6}$$

where $dz/dr_d = y$; note that when $r_d = 0$, $z = \delta$, $y = 0$, and $K = K_0$.

Equation (6) can be solved using the fourth-order Runge–Kutta method with any two initial input values consisting of the apex height δ, apex curvature K_0, or radial distance r_d.[19] In the calculation, the apex height δ and curvature K_0 are used as the only inputs. These two values are systematically varied to simultaneously match both the initial photoresist volume (assuming a 20% volume loss) and photoresist cylinder radius, which are defined by the photoresist coating and photolithography recipes. The final calculated photoresist droplet profile (dashed line) and the measured profile (solid line) are shown in Fig. 4. The lack of symmetry in the measured photoresist profile is due to artifacts introduced during the mechanical profilometer measurements.

C. Dry etch simulation

To achieve the final GaAs hemisphere, an ICP etch is performed after the photoresist reflow, in which the vertical and horizontal etch rates are carefully tuned. The photoresist reflow simulation results are an input for the etch simulation that is used to predict the etching result. In addition to the photoresist droplet profile, the etch calibration results are inputs for the simulation. From experiments the vertical etching selectivity between photoresist and GaAs is about 1:2.3 and the lateral etch rate is roughly one fifth of the corresponding vertical etch rate. Figure 5 shows the calculated and measured GaAs dome (nonperfect hemisphere) profile after etching. It can be seen that the top part of the etched dome is very close to a perfect hemisphere while the base deviates from the desirable curve.

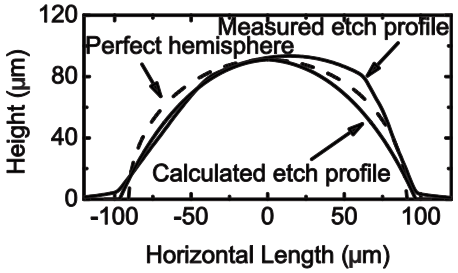

FIG. 5. Calculated and measured GaAs hemisphere (solid curves) compared to a perfect hemisphere (dashed curve).

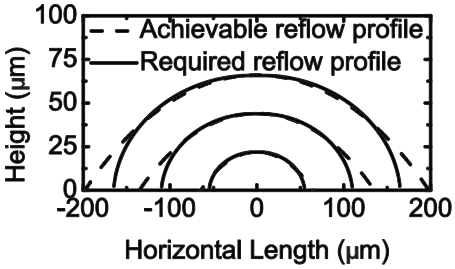

FIG. 6. Photoresist profiles (solid curves) required to etch perfect GaAs hemispheres and achievable photoresist profiles (dashed curves) for various photoresist droplet sizes.

To determine the ideal photoresist profile, simulations are performed starting from a perfect GaAs hemisphere and back calculating to what the profile should be. These calculations together with the measured photoresist profiles are shown in Fig. 6 for various photoresist droplet radii; which confirms that the measured photoresist profile is close to that required for a perfect hemisphere except near the edge of the base. Furthermore, as the radius gets smaller the measured and desired profiles are more closely matched. These numerical simulations confirm that spreading at the base of the reflowed photoresist droplet results in GaAs hemisphere profiles that are not perfect.

III. FABRICATION RESULTS

With the aid of theoretical simulations, the critical device fabrication steps are schematically shown in Fig. 7. First the active region is fabricated on the epitaxial layer with both n and p contacts formed on the active region side of the substrate. Next four windows are opened by etching down through the active layers to a depth of 15 μm. These windows serve as the etch stop detection point during the hemisphere etching from the backside of the substrate. Next the substrate is lapped and polished down to a thickness of about

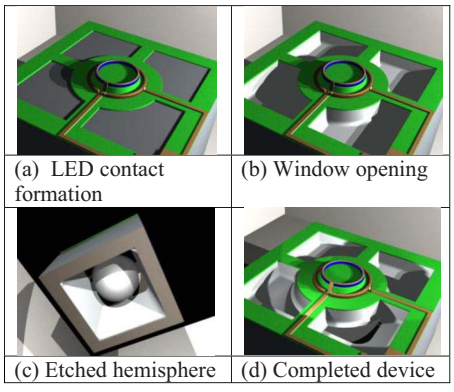

FIG. 7. (Color online) Schematic of the fabrication flow for the monolithic integration of a semiconductor hemisphere with light emitting active region.

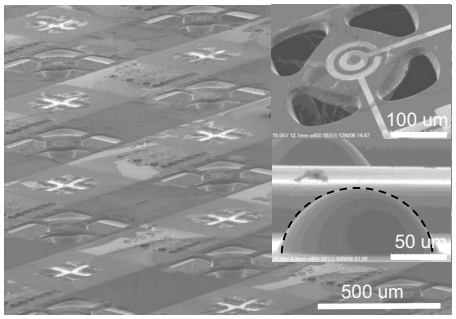

FIG. 8. Scanning electron micrographs of GaAs hemispheres integrated with InGaAs active regions.

120 μm. And finally the GaAs hemispheres, centered over the active region, are fabricated from the backside of the remaining substrate. Once the final etch is completed, four arms are formed that connect the active region and contacts to the surroundings.

To attain the correct hemisphere curvature and size, a 27 μm thick layer of AZ4620 photoresist is coated on the backside of the remaining substrate using multiple spin steps followed by standard photolithography to form a photoresist cylinder with a 100 μm radius. The photoresist cylinder is reflowed to create a domed photoresist mesa mask by slowly heating up the sample from 60 to 125 °C. The final profile is shown in Fig. 4 (solid curve). In this step the temperature is slowly increased to avoid creating any big air bubbles and slowly decreased to avoid photoresist cracking due to strain. An ICP etch is used to transfer the domed photoresist pattern onto the GaAs substrate to create the hemisphere. In the etch step, it is critical to etch away all the photoresist to avoid leaving a flat top on the GaAs hemisphere.

Scanning electron micrographs of fabricated devices are shown Fig. 8; these particular devices have hemispheres with a 90 μm radius and active regions with a 30 μm radius and the *p*-contact covers approximately 44% of the active area (design 1). The array of GaAs hemispheres are nearly perfect and highly uniform, which indicates the potential for large volume fabrication. Preliminary experiments show that this process is also applicable to other materials, such as Si, GaP, InP, and GaSb.

The overall size of the device is limited by the requirement of a nearly ideal reflowed photoresist droplet profile as a mask to etch near perfect hemispheres, see Fig. 6. Furthermore, the light extraction performance of a given hemisphere increases as the size of the active region decreases, see Fig. 2. Therefore, to achieve near perfect hemisphere devices with high extraction efficiency, the active region must be small, resulting a reduced power output per hemisphere and more hemispheres per device to achieve a given power output. Moreover, further increases in the extraction efficiency can be achieved by reducing the metal contact losses, through reduced contact ring area and by using contact materials that are more reflective.

As a comparison to our approach, micro lenses are traditionally categorized into two groups: (i) polymer or glass based and (ii) semiconductor based. Polymer based micro lenses are fabricated using reflow, hot/UV embossing, gray scale lithography, microjet technique, excimer laser ablation, and direct laser write techniques.[20–26] Although high aspect ratio lenses are possible, the refractive indices are typically not matched to the light emitting material. On the other hand, semiconductor based micro lenses are typically fabricated using focused ion beam or pattern transfer from photoresist to semiconductor by wet or dry etching.[27–35] The refractive indices are matched but only low aspect ratio micro lenses are typically achieved. Although high aspect ratio GaAs hemispheres have been attempted,[36] no design rules or detailed processing steps have been published and the large volume production capability was unclear.

IV. CONCLUSION

A semiconductor hemisphere is monolithically integrated with a light emitting active region for high light extraction efficiency. Near perfect semiconductor micro hemispheres are fabricated by photoresist reflow and ICP etching. Simulations show that with optimal designs the hemisphere structure can extract over 99.9% of the light incident upon it, which can result in realizable extraction efficiencies between 80% and 90%. Processing results show that arrays of GaAs hemispheres with good uniformity can be fabricated, indicating the potential for large volume fabrication.

ACKNOWLEDGMENTS

This work was supported by a MURI program from the (U. S.) Air Force Office of Scientific Research under Grant No. FA9550-04-1-0374. The authors would like to thank N. Rider for the 3D graphics.

[1]J. Tauc, Czech. J. Phys. **7**, 275 (1957).
[2]S.-Q. Yu, J.-B. Wang, D. Ding, S. R. Johnson, and Y.-H. Zhang, Solid-State Electron. **51**, 1387 (2007).
[3]M. Sheik-Bahae and R. I. Epstein, Phys. Rev. Lett. **92**, 247403 (2004).
[4]R. I. Epstein, M. I. Buchwald, B. C. Edwards, T. R. Gosnell, and C. E. Mungan, Nature (London) **377**, 500 (1995).
[5]D. V. Seletskiy, S. D. Melgaard, S. Bigotta, A. D. Lieto, M. Tonelli, and M. Sheik-Bahae, Nat. Photonics **4**, 161 (2010).
[6]J. Thiede, J. Distel, S. R. Greenfield, and R. I. Epstein, Appl. Phys. Lett. **86**, 154107 (2005).
[7]H. Luo, J. K. Kim, and E. F. Schubert, Appl. Phys. Lett. **86**, 243505 (2005).
[8]J. J. Wierer, A. David, and M. M. Megens, Nat. Photonics **3**, 163 (2009).
[9]I. Schnitzer, E. Yablonovitch, C. Caneau, T. J. Gmitter, and A. Scherer, Appl. Phys. Lett. **63**, 2174 (1993).
[10]D. Ding, S. R. Johnson, J.-B. Wang, S.-Q. Yu, and Y.-H. Zhang, Optical Society of America, Conference on Lasers and Electro-Optics, 2008-CLEO/QELS Technical Digest, 2008 (unpublished), Paper No. CThKK3.
[11]S. L. Chuang, *Physics of Optoelectronic Devices*, 1st ed. (Wiley-Interscience, New York, NY, 1995), pp. 205–213.
[12]E. D. Palik, *Handbook of Optical Constants of Solids*, 1st ed. (Academic, San Diego, CA, 1985), pp. 729.
[13]E. D. Palik, *Handbook of Optical Constants of Solids II*, 1st ed. (Academic, San Diego, CA 1991), pp. 770 and 790.
[14]Ü. Özgür, Ya. I. Alivov, C. Liu, A. Teke, M. A. Reshchikov, S. Doğan, V. Avrutin, S.-J. Cho, and H. Morkoç, J. Appl. Phys. **98**, 041301 (2005).
[15]W. G. Spitzer and J. M. Whelan, Phys. Rev. **114**, 59 (1959).
[16]V. A. Nemchinsky, J. Phys. D: Appl. Phys. **27**, 1433 (1994).
[17]HOECHST CELANESE Corporation, AZ4620 photoresist material safety data sheet.

[18]J. G. Speight, *Lange's Handbook of Chemistry*, 16th ed. (McGraw-Hill, New York, NY, 2005), pp. 226–230, 272–286.
[19]J. C. Butcher, *Numerical Methods for Ordinary Differential Equations*, 2nd ed. (Wiley, West Sussex, England, 2003), p. 90.
[20]Z. D. Popovic, R. A. Sprague, and G. A. Neville Connell, Appl. Opt. **27**, 1281 (1988).
[21]B.-K. Lee, K. J. Cha, and T. H. Kwon, Microelectron. Eng. **86**, 857 (2009).
[22]C. Y. Chang, S. Y. Yang, and J. L. Sheh, Microsyst. Technol. **12**, 754 (2006).
[23]J. D. Rogers, A. H. O. Karkkainen, T. Tkaczyk, J. T. Rantala, and M. R. Descour, Opt. Express **12**, 1294 (2004).
[24]E. Bonaccurso, H.-J. Butt, B. Hankeln, B. Niesenhaus, and K. Graf, Appl. Phys. Lett. **86**, 124101 (2005).
[25]K. Naessens, H. Ottevaere, P. Van Daele, and R. Baets, Appl. Surf. Sci. **208–209**, 159 (2003).
[26]J. Tan, M. Shan, C. Zhao, and J. Liu, Appl. Opt. **47**, 1430 (2008).
[27]Y. Fu and N. K. Bryan, IEEE Trans. Semicond. Manuf. **15**, 229 (2002).
[28]E. M. Strzelecka, G. D. Robinson, M. G. Peters, F. H. Peters, and L. A. Coldren, Electron. Lett. **31**, 724 (1995).
[29]M. Eisner and J. Schwider, Opt. Eng. **35**, 2979 (1996).
[30]T. N. Oder, J. Shakya, J. Y. Lin, and H. X. Jiang, Appl. Phys. Lett. **82**, 3692 (2003).
[31]Si-Hyun Park, Heonsu Jeon, Youn-Joon Sung, and Geun-Young Yeom, Appl. Opt. **40**, 3698 (2001).
[32]E. Gu, H. W. Choi, C. Liu, C. Griffin, J. M. Girkin, I. M. Watson, M. D. Dawson, G. McConnell, and A. M. Gurney, Appl. Phys. Lett. **84**, 2754 (2004).
[33]H. Nishiyama, J. Nishii, M. Mizoshiri, and Y. Hirata, Appl. Surf. Sci. **255**, 9750 (2009).
[34]C.-F. Chen, S.-D. Tzeng, H.-Y. Chen, and S. Gwo, Opt. Lett. **30**, 652 (2005).
[35]Y.-S. Kim, J. Kim, J.-S. Choe, Y.-G. Rob, H. Jeon, and J. C. Woo, IEEE Photonics Technol. Lett. **12**, 507 (2000).
[36]W. N. Carr and G. E. Pittman, Appl. Phys. Lett. **3**, 173 (1963).